Urban Forestry & Urban Greening 16 (2016) 208–220

Contents lists available at ScienceDirect

Urban Forestry & Urban Greening

journal homepage: www.elsevier.com/locate/ufug

The feasibility of remotely sensed data to estimate urban tree dimensions and biomass☆

Jun-Hak Lee [a,*], Yekang Ko [b], E. Gregory McPherson [c]

[a] Department of Earth and Environmental Sciences, University of Texas at Arlington, USA
[b] Department of Planning and Landscape Architecture, University of Texas at Arlington, USA
[c] USDA Forest Service, Pacific Southwest Research Station, USA

ARTICLE INFO

Article history:
Received 13 February 2015
Received in revised form 6 January 2016
Accepted 19 February 2016
Available online 28 February 2016

Keywords:
Aerial images
Crown diameter
DBH
LiDAR
Tree height
Urban tree biomass

ABSTRACT

Accurately measuring the biophysical dimensions of urban trees, such as crown diameter, stem diameter, height, and biomass, is essential for quantifying their collective benefits as an urban forest. However, the cost of directly measuring thousands or millions of individual trees through field surveys can be prohibitive. Supplementing field surveys with remotely sensed data can reduce costs if measurements derived from remotely sensed data are accurate. This study identifies and measures the errors incurred in estimating key tree dimensions from two types of remotely sensed data: high-resolution aerial imagery and LiDAR (Light Detection and Ranging). Using Sacramento, CA, as the study site, we obtained field-measured dimensions of 20 predominant species of street trees, including 30–60 randomly selected trees of each species. For each of the 802 trees crown diameter was estimated from the aerial photo and compared with the field-measured crown diameter. Three curve-fitting equations were tested using field measurements to derive diameter at breast height (DBH) ($r^2 = 0.883$, RMSE = 10.32 cm) from the crown diameter. The accuracy of tree height extracted from the LiDAR-based surface model was compared with the field-measured height (RMSE = 1.64 m). We found that the DBH and tree height extracted from the remotely sensed data were lower than their respective field-measured values without adjustment. The magnitude of differences in these measures tended to be larger for smaller-stature trees than for larger stature species. Using DBH and tree height calculated from remotely sensed data, aboveground biomass ($r^2 = 0.881$, RMSE = 799.2 kg) was calculated for individual tree and compared with results from field-measured DBH and height. We present guidelines for identifying potential errors in each step of data processing. These findings inform the development of procedures for monitoring tree growth with remote sensing and for calculating single tree level carbon storage using DBH from crown diameter and tree height in the urban forest.

1. Introduction

Accurate data on the biophysical dimensions of individual trees such as diameter at breast height (DBH), height, crown diameter, and biomass are essential for quantifying the economic value, social benefits, and ecological services of the urban forest. Over the past few decades, numerous studies have quantified the benefits of urban forests. These ecosystem services include the reduction of atmospheric carbon dioxide (Nowak et al., 2013; Nowak and Crane, 2002; Rowntree and Nowak, 1991), absorption of air pollutants (Morani et al., 2011; Nowak et al., 2006; Scott et al., 1998), savings of space-conditioning energy in buildings (Donovan and Butry, 2009; Ko and Radke, 2014; McPherson and Rowntree, 1993; Simpson and McPherson, 1998), mitigation of the urban heat island (Deng and Wu, 2013; Huang et al., 1987; McPherson, 1994; McPherson and Muchnick, 2005; Roberts et al., 2012; Weng, 2009), outdoor thermal comfort (Shashua-Bar et al., 2011) and reduction of stormwater runoff (Xiao et al., 1998). Other studies have assessed social and economic benefits, such as mental and physical health improvement (Donovan et al., 2013; Gidlöf-Gunnarsson and Öhrström, 2007; Kaplan and Kaplan, 1989; van den Berg et al., 2010), crime reduction (Kuo and Sullivan, 2001; Schroeder and Anderson, 1984), and increased property values (Anderson and Cordell, 1988; Sander et al., 2010). As more people recognize the value of these services it

☆ The use of trade or firm names in this publication is for reader information and does not imply endorsement by the U.S. Department of Agriculture of any product or service.

* Corresponding author at: 119 Geoscience Building, Box 19049, 500 Yates Street, Arlington, TX 76019, USA. Tel.: +1 817 272 9365.
E-mail address: junhak@uta.edu (J.-H. Lee).

http://dx.doi.org/10.1016/j.ufug.2016.02.010
1618-8667/

becomes increasingly important to develop accurate and economical methods for measuring trees' dimensions and quantifying their performance.

In the past decade, remotely sensed data with high spatial resolution has been used to supplement field measurements of forest stand structure and tree dimensions. Aerial photographs and photogrammetric techniques have been used to measure forest parameters such as species, size, canopy density, and number of trees (Gong et al., 1999; Spurr, 1960). In particular, photogrammetric measurements have become popular for extracting precise forest information, even at the level of individual trees, due to their high spatial resolution and accuracy (Dralle and Rudemo, 1997; Korpela, 2004; Larsen and Rudemo, 1998). Several studies have developed automated approaches to extract individual tree canopy from high spatial resolution digital images, but these automated approaches are most applicable on forest areas with uniform patterns and distinctive tree canopies (Culvenor, 2002; Gougeon, 1995; Gougeon and Leckie, 2006; Ke and Quackenbush, 2011; Wang et al., 2004; Wulder et al., 2000). In the case of heterogeneous urban areas, however, with many species of trees in a non-uniform distribution, human interpreters more effectively recognize tree objects than automated programs (Nowak, 1993; Nowak and Greenfield, 2012; Parlin, 2009). Recently, Light Detection and Ranging (LiDAR) technology is garnering attention because of the capability of extracting both horizontal and vertical information at high spatial resolutions using airborne (Alonzo et al., 2015; Hyyppä et al., 2008, 2004; Koch and Dees, 2008; Lim et al., 2003) and ground-based system (Lefsky and McHale, 2008; McHale et al., 2009). Combined with hyperspectral imagery, LiDAR data can provide detailed species information in complex urban areas (Alonzo et al., 2014). Remote sensing techniques have been used with plot-based estimates of carbon storage to quantify and map urban forest carbon stocks citywide (McPherson et al., 2013).

While recent remote-sensing techniques provide useful information on the structure, function and value of urban tree canopy, it remains unclear how errors propagate during the process of estimating individual tree dimensions and biomass using remotely sensed data (e.g., airborne digital images, aerial photos, and LiDAR). If remote sensing can serve as an effective supplement to field surveyed data, it could make monitoring more economical by reducing the frequency of field measurements. The accuracy of tree dimensions measured with remote sensing are influenced by errors that occur during each step of the calculation. For example, correctly locating the target tree for measurement can be a possible source of error when its location is not accurately noted because falsely matched tree information could affect the model calibration and validation. Classification or digitizing the tree crown (e.g., aerial image interpretation) is a major source of error due to difficulties separating the overlapping boundaries of tree crowns (Richardson and Moskal, 2014). Additional uncertainty is added with use of regression models to estimate tree dimensions such as DBH, which cannot be directly measured from airborne remotely sensed data (Mäkinen et al., 2006). Each step in the process can amplify the error of the estimated tree dimension. Given this challenge, it is imperative to assess the accuracy of estimated dimensions before they are used to calculate tree biomass, carbon storage or other urban forest functions.

This study aims to assess the accuracy of remotely sensed data for measuring urban tree dimensions and biomass. We identify and measure errors obtained at each step of the estimation process to (1) determine crown diameter, DBH and tree height from aerial photographs and LiDAR imagery and (2) calculate aboveground biomass using estimated DBH, tree heights, and allometric equations from each species (Fig. 1). Estimated tree dimensions are compared with actual dimensions obtained from field measurements of 818 trees comprising the 20 predominant street tree

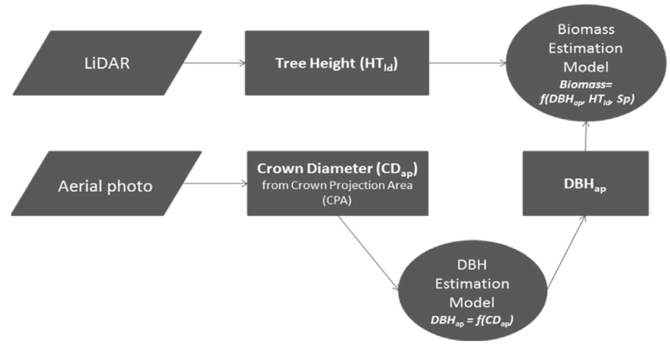

Fig. 1. Research design.

species (Table 1) in Sacramento, CA. For each tree we digitize the crown projection area (CPA), calculate the crown diameter (CD_{ap}), and compare it with field measured crown diameter. Using field measured data, we test three curve-fitting equations to establish relations between field measured crown diameter and DBH for each of the 20 sampled species, and identify the equation yielding the lowest error for each species. We apply the relevant equation to the remotely sensed CPA for each tree and calculate its diameter at breast height (DBH_{ap}). Similarly, the accuracy of each tree's estimated height is determined by comparing the field measured value with height extracted from a LiDAR-based surface model (HT_{ld}). These DBH_{ap} and HT_{ap} values are used with species-specific allometric equations to calculate each tree's aboveground biomass, which is compared to results from the field-measured DBH and height. It is important to note that we used publically available remotely sensed data that were not ideal. The LiDAR data were acquired during leaf-off condition and a time gap of several years exists between the time LiDAR was acquired and field measurements were recorded. However, these limitations are not unique to this study, and could be encountered by other cities and researchers interested in estimating the biophysical parameters and biomass of local trees. The effectiveness and limitations of the remote sensing-based measurements, biometric models and the resulting errors are discussed. We conclude that remotely sensed data can be a viable alternative to field measurements if the accuracies of derived tree dimensions are quantitatively assessed. These results will assist cities, consultants and others develop procedures to routinely monitor and measure tree dimensions with accepted levels of accuracy. When combined with periodic field surveys, this approach may reduce the cost of monitoring compared to solely relying on traditional field surveys.

2. Methods

2.1. Study area

The City of Sacramento covers 253.61 km^2 (38°33′20″N 121°28′8″W, Fig. 2) and has a population of 466,488, making it the 35th most populous city in the United States (US Census Bureau, 2014). Sacramento's Mediterranean climate is characterized by wet, mild winters and hot, dry summers. The average low temperature in January is 3.3 °C while the average high temperature in July is 33.9 °C. On average, 74 days a year are above 32.2 °C (90 °F) (City of Sacramento, 2012).

Sacramento's urban forest is nationally renowned because of its rich history (McPherson and Luttinger, 1998) and successful partnerships among local agencies, utilities and non-profits. American Forests, for example, selected the City of Sacramento as having one of the 10 best urban forests in the United States (American Forests, 2014). Urban tree canopy is 18.2% and there are approximately 6.9

million trees in the Sacramento region (McPherson et al., 2013). The city's Urban Forestry section manages 115,000 trees in street rights-of-way, parks, and other city facilities (American Forests, 2014). Nowak and Crane (2002) estimated that the carbon density in Sacramento was very high (46.9 tC/ha; 36.1 kgC/m^2 cover) compared to that of nine other US cities in their study, possibly due to its extensive and mature urban forest (McPherson, 1998).

2.2. Data

2.2.1. Field measurements

We obtained field-measured dimensions of 818 Sacramento street trees from the US Forest Service (McPherson and Peper, 2012). The stratified random sample of 20 predominant tree species consisted of 19–61 individual trees of each species (Table 1). The sample for each species was stratified by DBH class so that at least one and no more than ten trees in each class were included (up to nine classes for the largest species). Measurements included DBH (to the nearest 0.1 cm), and tree height (HT), height to crown base, and crown height (all to the nearest 0.5 m). Crown diameter (CD) was measured in two directions (parallel and perpendicular to nearest street) to the nearest 0.5 m with a sonar measuring device. Tree age, defined as the number of years after planting, was determined from a combination of city records and historical data (McPherson and Peper, 2012).

Typically, equations to predict DBH from age, and to predict tree height, crown height, crown diameter, and leaf area from DBH, are developed using least-squares linear and non-linear regressions to determine best fit. Although site-specific environmental factors (such as microclimate, soil, and water) and human management (such as pruning) can cause individual urban trees of identical age or DBH to differ widely in height, crown diameter, and leaf area, these statistical methods try to identify broad trends in a sample. Over 1800 equations have been developed for 16 US reference cities to predict the growth of street trees and to estimate the benefits and costs associated with street tree populations; some of these equations have been published for California's San Joaquin Valley and Southern Coastal regions (Peper et al., 2001a, 2001b).

2.2.2. NAIP imagery

We used a set of Digital Ortho-rectified Images produced by the National Agricultural Imagery Program (NAIP) in 2010. We obtained the ortho-images from the California Spatial Information Library. The images contained multispectral 4-bands (red, green, blue and near infrared) with one-meter pixel resolution and were formatted to the Universal Transverse Mercator (UTM) geographic coordinate system using the North American Datum (NAD83). The ortho-imagery was rectified to a horizontal accuracy within 5 m of reference digital ortho quarter quads.

2.2.3. LiDAR data

We processed two existing LiDAR data sets from 2007 and 2008 to cover the City of Sacramento (Fig. 2). The first LiDAR dataset covered the Lower Sacramento River Study Area under the Central Valley Flood Plain Evaluation and Delineation project, for the California Department of Water Resources. The dataset was acquired in March 2008 and the data processing was completed in 2010. LiDAR data were collected at a density of 1.0 point per square meter, using a Leica ALS50-II sensor flown at an average flight height of 1219 m above mean sea level and an average sidelap of 30%. Up to four returns were recorded for each pulse in addition to an intensity value. The deliverable coordinate system was UTM Zone 10 Feet NAD83, with a vertical datum of NAVD 1988 Potterfield Geoid. The second dataset was obtained from the LiDAR flights of the Sacramento-San Joaquin Delta conducted during late January and February of 2007. The data were collected at 0.787 points per square meter utilizing an Optech ALTM-3100 sensor flown at an altitude of 1676 m and an average sidelap of 40%. All data were registered to UTM Zone 10, NAD83, vertical datum NAVD88. We should note that both sets of LiDAR data were obtained in winter months, when deciduous trees were dormant and leafless. The crown projection area of deciduous trees is harder to estimate accurately when trees are out of leaf than when they are in leaf.

2.3. Crown measurements using the NAIP images

We obtained crown measurements by digitizing crown boundaries from the NAIP imagery using ArcGIS 10.0 (ESRI). We used both false-color-composite (near infrared, red, and green) and natural-color (red, green, and blue) images to determine the boundary of individual trees. We determined the locations of the field-measured trees in the NAIP images based on the description of the tree location from the field survey. Photographs taken during the field survey also offered supplementary information used to verify that

Table 1
Summary statistics of sample trees: 20 predominant street tree species in Sacramento, CA.

Code	Scientific name	Common name	DBH (cm)					Tree height (m)			
			n	Mean	Min	Max	Std.	Mean	Min	Max	Std.
CEDE	*Cedrus deodara*	Deodar cedar	49	65.4	6.2	133.0	33.8	20.0	2.8	30.2	6.9
CEOC	*Celtis occidentalis*	Northern hackberry	28	41.4	11.7	94.6	21.5	11.5	4.8	22.8	4.6
CESI4	*Celtis sinensis*	Chinese hackberry	49	51.9	5.7	125.0	27.4	12.3	2.8	24.4	4.8
CICA	*Cinnamomum camphora*	Camphor tree	50	61.1	7.6	135.8	34.1	13.9	3.0	26.2	5.6
FRVEG	*Fraxinus velutina modesto*	Modesto ash	36	59.4	4.4	145.5	30.2	12.7	4.0	23.0	4.2
GIBI	*Ginkgo biloba*	Ginkgo	54	47.5	4.7	110.0	23.6	14.9	3.0	30.2	6.2
LAIN	*Lagerstroemia indica*	Common crape myrtle	24	20.6	7.6	40.9	10.1	6.3	3.0	10.0	1.6
LIST	*Liquidambar styraciflua*	Sweetgum	37	44.5	4.1	120.5	24.7	16.9	3.5	33.0	7.1
LITU	*Liriodendron tulipifera*	Tulip tree	46	60.0	5.0	140.8	32.4	20.6	3.2	35.2	7.6
MAGR	*Magnolia grandiflora*	Southern magnolia	58	49.6	6.0	95.6	21.8	12.8	4.0	22.6	4.3
PICH	*Pistacia chinensis*	Chinese pistache	34	40.0	4.8	72.8	17.8	12.3	3.8	19.0	3.9
PLAC	*Platanus × acerifolia*	London planetree	41	56.1	9.3	133.9	32.7	17.2	5.0	36.0	8.2
PRCE	*Prunus cerasifera* spp.	Cherry plum	19	26.9	9.5	36.9	8.8	6.6	3.3	9.8	2.0
PYCA	*Pyrus calleryana* spp.	Callery pear	30	30.1	6.3	56.6	13.9	11.1	4.5	18.5	4.0
QUAG1	*Quercus agrifolia*	Coastal live oak	45	47.2	6.2	97.7	22.4	11.8	2.6	19.8	4.4
QULO	*Quercus lobata*	California white oak	44	59.9	7.7	135.6	37.3	15.2	6.5	27.0	5.5
QURU	*Quercus rubra*	Northern red oak	32	41.9	3.5	101.6	26.4	14.7	4.0	26.0	6.7
SESE	*Sequoia sempervirens*	Coast redwood	41	69.2	8.7	173.1	49.1	19.2	4.5	36.0	10.0
ULPA	*Ulmus parvifolia*	Chinese elm	47	54.3	8.2	98.2	22.0	15.4	4.0	24.8	5.3
ZESE	*Zelkova serrata*	Japanese zelkova	38	53.1	5.1	114.3	29.4	13.9	4.2	26.0	5.6
All			802	51.2	3.5	173.1	30.3	14.5	2.6	36.0	6.8

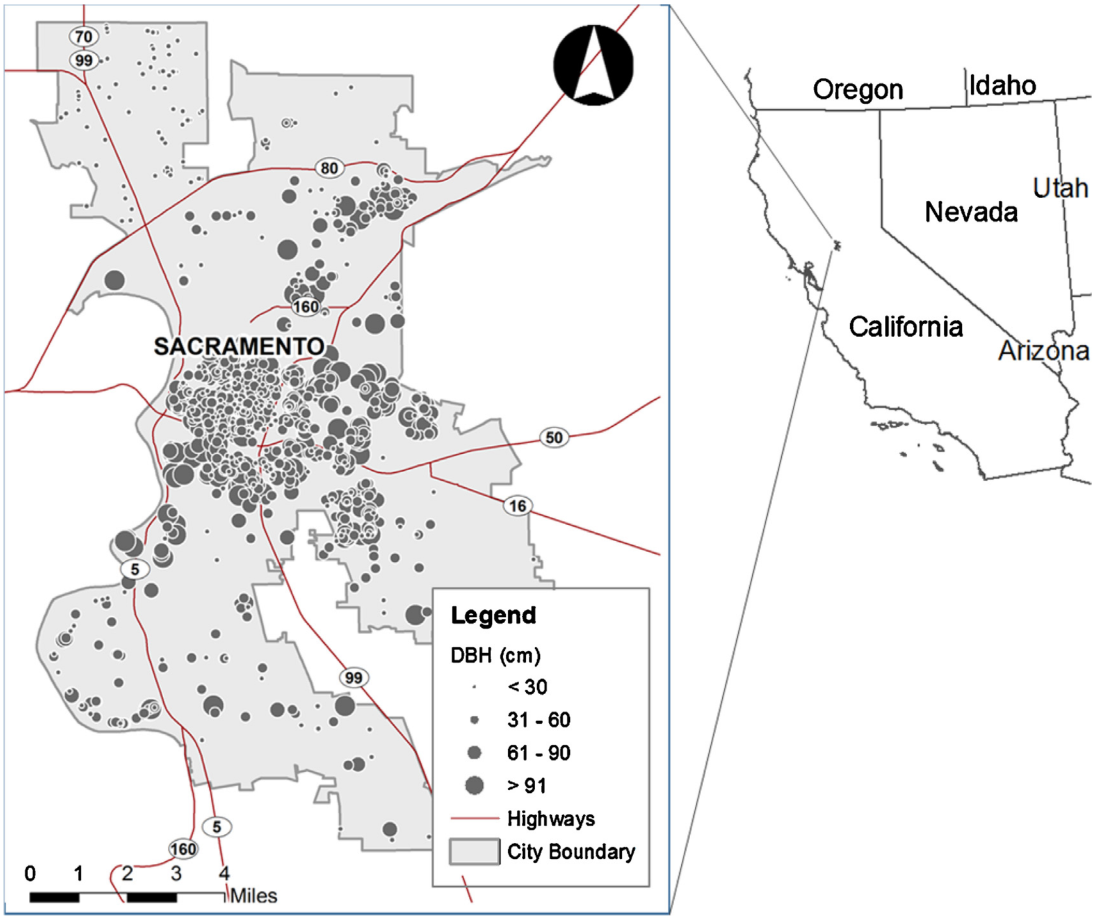

Fig. 2. Overview of study area (City of Sacramento boundary). Circles show the location of field measured trees (size of circle is proportional to tree DBH).

the field-measured trees were the same ones identified in the NAIP images. Once we had determined the corresponding tree in the NAIP image, we carefully delineated the crown boundary from the ortho-images. It should be noted that there are limitations to manual interpretation. For example, although we used ortho-images, not all images were perfectly ortho-rectified. Some of the images showed building façades that would not be visible in properly rectified aerial photos (Mäkinen et al., 2006). Although the LiDAR data had better geometric accuracy than the NAIP imagery, we used the NAIP imagery because it was acquired during the leaf-on season, thus better representing the real crown area. Digitized crown boundaries also had errors because some were too fuzzy to clearly distinguish boundaries. In the case of clumped trees with contiguous canopies, it was challenging to draw a clear distinction between each tree's crowns. Although the same person digitized all the crown boundaries, some decisions relied on the researchers' interpretation. Each tree's crown projection area (CPA) was calculated from the digitized crown boundary recorded in the GIS (Geographic Information System). We calculated an average crown radius (m) from CPA and converted to crown diameter by multiplying by two. This conversion assumed that tree crowns were circular, an assumption supported for open growing trees (McPherson and Rowntree, 1988; Wilkinson, 1995) but not tightly clustered trees.

2.4. Tree height estimation using LiDAR data

Because the NAIP imagery provided two-dimensional information only (i.e., CPA), we extracted tree heights from the LiDAR surfaces. This was accomplished by subtracting the elevation value of the ground at the treetop location in DEM from the treetop elevation value in DSM. This LiDAR-based method reduced potential estimation error compared to indirectly estimating tree heights using allometric equations that were based on estimated crown diameter and DBH. Also, allometric estimations may not account for the effects of pruning on tree height. Crown reduction pruning is undertaken when trees grow into overhead power lines, street lights, traffic signals and signs.

Treetops were first detected from the Digital Surface Model (DSM) derived from LiDAR points. We converted discrete LiDAR points to a regular grid. We laid out a grid and assigned the maximum value within each cell as a cell value to derive the top of the surface with 1 m cell size (Popescu and Wynne, 2004). After linear interpolation was performed, 2D Gaussian filter was applied to smooth the DSM. Then, we use the extended-maxima transform, which is a useful method to detect peaks ("maximal structure") in the canopy surface model (Chen et al., 2006; Kwak et al., 2007; Lee, 2010). Extended-maxima transformation is the regional maxima of the H-maxima transformation that suppresses all maxima whose height or depth does not exceed a given threshold level h (here, $h = 0.5$ m) (Chen et al., 2006; Kwak et al., 2007; Lee, 2010). Fig. 3 illustrates an example of the extended-maxima transformation (Lee, 2010). Because the result of extended maxima transformation was a region (connected cells), the maximum elevation value in the region of the DSM was selected as a treetop. Here, these "detected blobs" include the peaks of tree crowns and the partial roof planes of buildings. We selected detected blobs that were within the digitized crown boundaries and classified them as treetops. When multiple treetop points existed within a crown boundary, we chose the maximum elevation value for our calculation of the tree's height. Finally, we obtained tree heights by

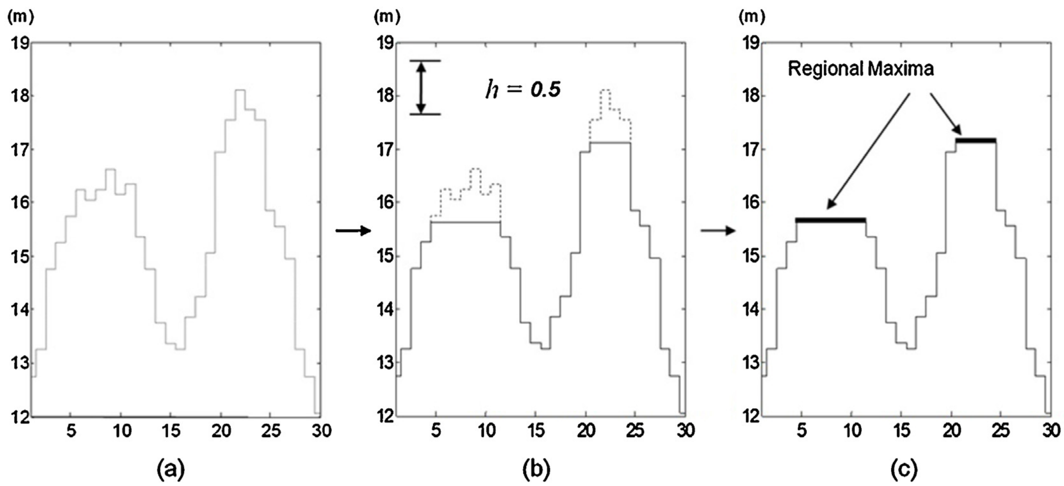

Fig. 3. An example of extended-maxima transformation. (a) Digital Surface Model. (b) H-maxima transformation (solid line) of the DSM (dashed line). (c) Extracting regional maxima (thick solid line) from the H-maxima transformed image (solid line).

subtracting the elevation value of ground at the treetop location in Digital Elevation Model (DEM) from the treetop elevation value in DSM.

2.5. Regression model to estimate DBH from crown radius by species

Three fitting models were tested to estimate DBH from crown diameter by species: one linear model (Eq. (1)) and two nonlinear models (Eqs. (2) and (3)). Dawkins (1963) found that relationships between crown diameters and stem diameters of trees are close to being linear when the DBH range is 20–50 cm (Hemery et al., 2005). Mugo et al. (2011) found that the linear model is the best to estimate DBH from crown diameters for three out of the five species tested. Lockhart et al. (2005) argued that the linear model provided the best model fit for estimating DBH from mean crown radius for six hardwood species. Popescu (2007) applied a linear relationship to estimate DBH from LiDAR-driven crown diameter and tree height. Kalliovirta and Tokola (2005) predicted DBH using crown diameter with a square root transformed curve fitting model (Eq. (2)). Korpela et al. (2007) applied this model to estimate DBH using the crown diameter measurement from aerial images. Chen et al. (2007) tested the univariate power models to estimate basal area (or DBH) from crown diameter based on basic allometric relationships found in plant sciences (Enquist, 2002; West et al., 1999). Although it is possible to estimate DBH directly from crown diameter from aerial image, we intentionally separated this into two steps – (1) crown measurements from aerial images and (2) predicting DBH from crown diameters so that the regression models (estimating DBH from crown diameter) for different tree species are available to other studies.

$$\mathrm{DBH}_i = a \times \mathrm{CD}_i + b \tag{1}$$

$$\sqrt{\mathrm{DBH}_i} = a \times \sqrt{\mathrm{CD}_i} + b \tag{2}$$

$$\mathrm{DBH}_i = a \times \mathrm{CD}_i^b \tag{3}$$

where DBH_i is the diameter at breast height for species "*i*", CD_i the crown diameter for species "*i*", and *a* and b are the parameters to be estimated.

For each of the 20 species described above, we checked normality and homoscedasticity assumptions for the models by using the Box-Cox method (Draper, 1998). If a model violated our assumptions, we dropped that model, regardless of goodness of fit. We calculated the root mean squared error of estimation (RMSE) and the coefficient of determination (R^2) to evaluate goodness of fit. Based on the model's goodness of fit, we determined the best model to predict DBH from crown diameter (Anderson-Sprecher, 1994; Chen et al., 2007). We used 10-fold cross-validation to minimize the underestimation of the prediction errors due to the usage of the same data for the training and testing (Rozeboom, 1978; Shrestha and Wynne, 2012; Stone, 1974; Zhang, 1997).

2.6. Aboveground biomass estimation from the remotely sensed data by species

Accurate biomass estimation is critical to assessing carbon storage in trees because they are directly proportional to each other. Allometric equations are commonly used to calculate biomass from DBH and tree height (Jenkins et al., 2003; Niklas, 1994). We calculated the biomass of individual trees with two scenarios from the remotely sensed data: (1) using only DBH_{ap} estimated from the aerial photo and (2) using DBH_{ap} and tree heights measured from LiDAR data (TH_{ld}) (McHale et al., 2009). We used 10-fold cross-validation for the accuracy assessment of biomass estimation (Rozeboom, 1978; Shrestha and Wynne, 2012). We compared these remotely sensed estimations of biomass to the results calculated from the field-measured DBH and tree height. We then selected allometric equations for each species using the following hierarchy: (1) urban-derived equations for the species and (2) forest-derived equations for the region. Tables 2 and 3 show (1) the equations for biomass estimation using DBH only and (2) the equations for biomass estimation using DBH and height, respectively. We carefully identified outliers using jackknife residuals for biomass estimation by species (Kleinbaum and Nizam, 2008; Shrestha and Wynne, 2012). We examined every outlier and excluded an outlier only if we could clearly justify its cause.

3. Results

3.1. Crown diameter estimation accuracy from aerial images

We assessed the accuracy of crown diameters extracted from the NAIP images by comparing them with the field-measured crown diameters for each species. Additionally, we calculated the mean and standard deviation of the differences between the crown diameters from aerial imagery and those from field measurements ($\mathrm{CD}_{fm} - \mathrm{CD}_{ap}$) (Fig. 4). For all species, mean crown diameters from aerial images were lower than field-measured diameters, and

Table 2
Equations for biomass estimation using DBH only.

Scientific name	Equations	Sources
Cedrus deodara	$=(\exp(-2.0336+2.2592\times\ln(\text{dbhcm}))-\exp(-2.9584+(4.4766/\text{dbhcm})))$	Jenkins et al. (2004)[a]
Celtis occidentalis	$=0.0014159\times\text{dbhcm}^{1.928}$	McHale (2007)
Celtis sinensis	$=0.0014159\times\text{dbhcm}^{1.928}$	McHale (2007)
Cinnamomum camphora	$=0.0283168466(0.031449\times(\text{dbhcm}/2.54)^{2.534660})$	Pillsbury et al. (1998)
Fraxinus velutina modesto	$=0.0283168466(0.022227\times(\text{dbhcm}/2.54)^{2.633462})$	Pillsbury et al. (1998)
Ginkgo biloba	$=0.000283509\times\text{dbhcm}^{2.310647}$	Aguaron and McPherson (2012)
Lagerstroemia indica	$=0.000283509\times\text{dbhcm}^{2.310647}$	Aguaron and McPherson (2012)
Liquidambar styraciflua	$=0.0283168466(0.030684\times(\text{dbhcm}/2.54)^{2.560469})$	Pillsbury et al. (1998)
Liriodendron tulipifera	$=0.000283509\times\text{dbhcm}^{2.310647}$	Aguaron and McPherson (2012)
Magnolia grandiflora	$=0.0283168466(0.022744\times(\text{dbhcm}/2.54)^{2.622015})$	Pillsbury et al. (1998)
Pistacia chinensis	$=0.0283168466(0.019003\times(\text{dbhcm}/2.54)^{2.808625})$	Pillsbury et al. (1998)
Platanus × acerifolia	$=0.0283168466(0.025170\times(\text{dbhcm}/2.54)^{2.673578})$	Pillsbury et al. (1998)
Prunus cerasifera spp.	$=0.000283509\times\text{dbhcm}^{2.310647}$	Aguaron and McPherson (2012)
Pyrus calleryana spp.	$=0.000283509\times\text{dbhcm}^{2.310647}$	Aguaron and McPherson (2012)
Quercus agrifolia	Not available – dbh and ht only	
Quercus lobata	Not available – dbh and ht only	
Quercus rubra	$=(0.1130\times(\text{dbhcm}^{2.4572}))-(\exp(-4.0813+(5.8816/\text{dbhcm})))$	Ter-Mikaelian and Korzukhin (1997)
Sequoia sempervirens	$=(\exp(-2.0336+2.2592\times\ln(\text{dbhcm}))-\exp(-2.9584+(4.4766/\text{dbhcm})))$	Jenkins et al. (2004)[a]
Ulmus parvifolia	$=0.0048879\times\text{dbhcm}^{1.613}$	McHale (2007)
Zelkova serrata	$=0.0283168466(0.021472\times(\text{dbhcm}/2.54)^{2.674757})$	Pillsbury et al. (1998)

Source: Peper, P. US Forest Service.
[a] Modified from Jenkins et al. (2004)'s equation by excluding foliar biomass.

Table 3
Equations for biomass estimation using DBH and tree height.

Scientific name	Equations	Sources
Cedrus deodara	$=(\exp(-2.0336+2.2592\times\ln(\text{dbhcm}))-\exp(-2.9584+(4.4766/\text{dbhcm})))$	Jenkins et al. (2004)[a]
Celtis occidentalis	$=0.002245\times\text{dbhcm}^{2.118}\times\text{htm}^{-0.447}$	McHale et al. (2007)
Celtis sinensis	$=0.002245\times\text{dbhcm}^{2.118}\times\text{htm}^{-0.447}$	McHale et al. (2007)
Cinnamomum camphora	$=0.0283168466\times(0.00982\times(\text{dbhcm}/2.54)^{2.13480}\times(3.28\times\text{htm})^{0.63404})$	Pillsbury et al. (1998)
Fraxinus velutina modesto	$=0.0283168466(0.00129\times(\text{dbhcm}/2.54)^{1.76296}\times(3.28\times\text{htm})^{1.42782})$	Pillsbury et al. (1998)
Ginkgo biloba	$=0.000196665\times\text{dbhcm}^{1.951853}\times\text{htm}^{0.664255}$	Aguaron and McPherson (2012)
Lagerstroemia indica	$=0.000196665\times\text{dbhcm}^{1.951853}\times\text{htm}^{0.664255}$	Aguaron and McPherson (2012)
Liquidambar styraciflua	$=0.0283168466\times(0.01177\times(\text{dbhcm}/2.54)^{2.31582}\times(3.28\times\text{htm})^{0.41571})$	Pillsbury et al. (1998)
Liriodendron tulipifera	$=0.000196665\times\text{dbhcm}^{1.951853}\times\text{htm}^{0.664255}$	Aguaron and McPherson (2012)
Magnolia grandiflora	$=0.0283168466\times(0.00449\times(\text{dbhcm}/2.54)^{2.07041}\times(3.28\times\text{htm})^{0.84563})$	Pillsbury et al. (1998)
Pistacia chinensis	$=0.0283168466(0.00292\times(\text{dbhcm}/2.54)^{2.19157}\times(3.28\times\text{htm})^{0.94367})$	Pillsbury et al. (1998)
Platanus × acerifolia	$=0.0283168466\times(0.01043\times(\text{dbhcm}/2.54)^{2.43642}\times(3.28\times\text{htm})^{0.39168})$	Pillsbury et al. (1998)
Prunus cerasifera spp.	$=0.000196665\times\text{dbhcm}^{1.951853}\times\text{htm}^{0.664255}$	Aguaron and McPherson (2012)
Pyrus calleryana spp.	$=0.000196665\times\text{dbhcm}^{1.951853}\times\text{htm}^{0.664255}$	Aguaron and McPherson (2012)
Quercus agrifolia	$=0.0283168466\times(0.0065261029\times(\text{dbhcm}/2.54)^{2.31958}\times(3.28\times\text{ht})^{0.62528})$	Pillsbury and Kirkley (1984)
Quercus lobata	$=0.0283168466\times(0.005887\times(\text{dbhcm}/2.54)^{1.94165}\times(3.28\times\text{htm})^{0.86562})$	Pillsbury and Kirkley (1984)
Quercus rubra	$=(0.1130\times(\text{dbhcm}^{2.4572}))-(\exp(-4.0813+(5.8816/\text{dbhcm})))$	Ter-Mikaelian and Korzukhin (1997)
Sequoia sempervirens	$=(\exp(-2.0336+2.2592\times\ln(\text{dbhcm}))-\exp(-2.9584+(4.4766/\text{dbhcm})))$	Jenkins et al. (2004)[a]
Ulmus parvifolia	$=0.000338\times\text{dbhcm}^{0.855}\times\text{htm}^{2.041}$	McHale et al. (2007)
Zelkova serrata	$=0.0283168466(0.00666\times(\text{dbhcm}/2.54)^{2.36318}\times(3.28\times\text{htm})^{0.55190})$	Pillsbury et al. (1998)

Source: Peper, P. US Forest Service.
[a] Modified from Jenkins et al. (2004)'s equation by excluding foliage biomass.

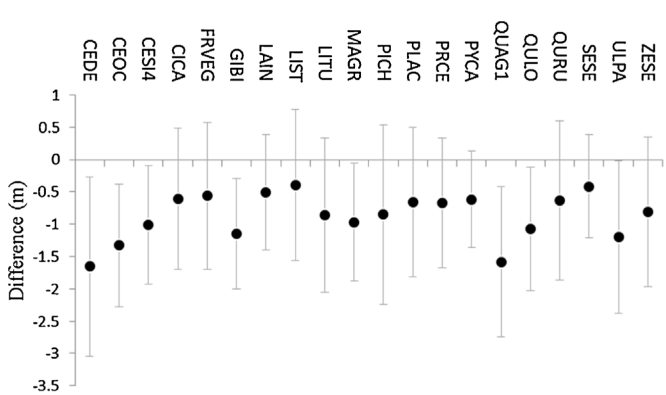

Fig. 4. Mean and standard deviations for the differences between the estimated crown diameters from aerial images and field measured crown diameters (by tree species).

for some species the derived diameters were always lower than measured diameters. Therefore, we adjusted the crown diameter estimation by using linear regression models between CD_{ap} and CD_{fm} by species (Eq. (4)). Fig. 5(a) and Table 4 show RMSE of crown diameter estimation from aerial images for 20 tree species. Before the adjustment, RMSE for all trees was 1.43 m (12.0%) and varied from 0.89 m (*Sequoia sempervirens*, SESE) to 2.15 m (*Cedrus deodara*, CEDE). After the adjustment, overall RMSE for all trees was reduced to 1.07 m. Although RMSEs (m) show a positive relationship with the mean crown diameters, trees with smaller crown diameters tended to have larger RMSE percentage values as expected. The small crape myrtle (*Lagerstroemia indica*, LAIN) showed the largest RMSE (15.0%) among 20 species, while the very large valley oak (*Quercus lobata*, QULO) had the smallest RMSE (6.6%).

$$CD_{adj} = a \times CD_{ap} + b \tag{4}$$

where CD_{adj} is the adjusted crown diameter and CD_{ap} is the crown diameter from aerial image.

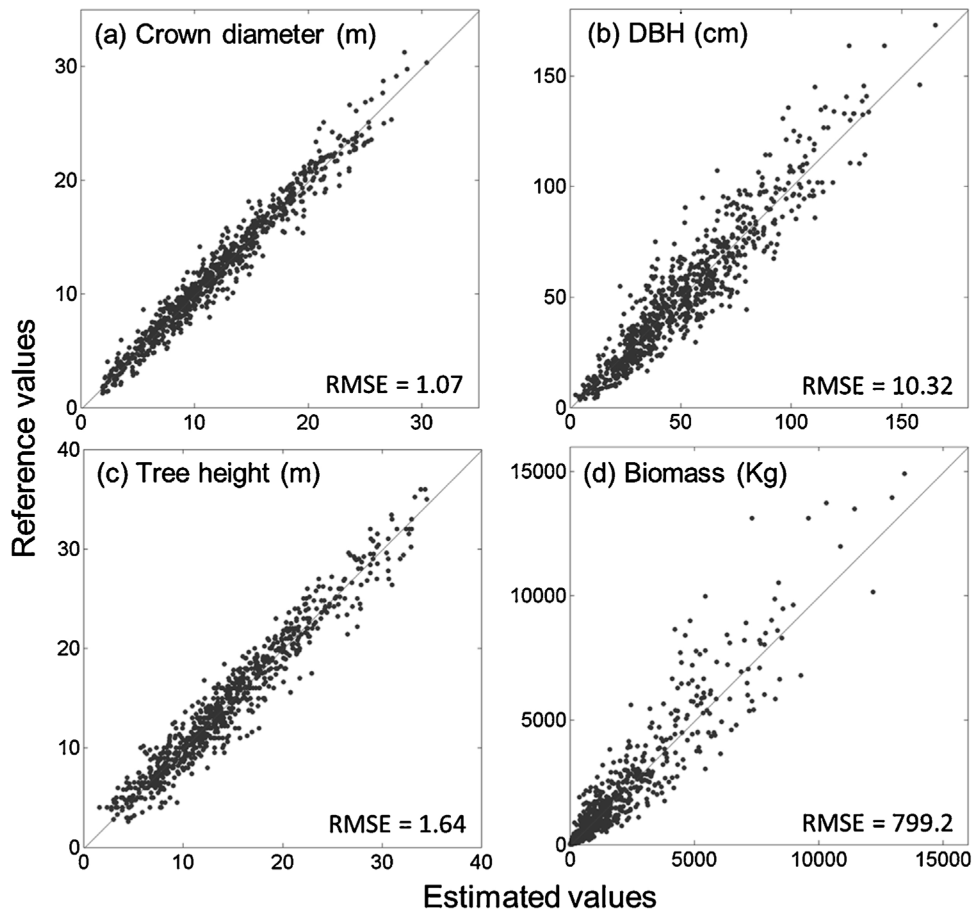

Fig. 5. Relationship between (a) field-measured crown diameters and the same measurements using aerial images, (b) field-measured DBH and estimated DBH using aerial image, (c) field-measured tree height and the same measurements from airborne LiDAR data, and (d) calculated biomass from field measurements and estimated biomass from the remotely sensed data.

Table 4
RMSEs of crown diameter estimation of 20 tree species from aerial images.

Species	Scientific name	# trees	Mean CD	RMSE (before adjust)		Adjustment		RMSE (after adjust)	
			(m)	(m)	(%)	*a*	*b*	(m)	(%)
CEDE	*Cedrus deodara*	49	12.93	2.15	16.6%	1.17	−0.22	1.13	8.7%
CEOC	*Celtis occidentalis*	28	12.27	1.62	13.2%	1.08	0.50	0.86	7.0%
CESI4	*Celtis sinensis*	49	13.39	1.36	10.1%	1.00	1.01	0.91	6.8%
CICA	*Cinnamomum camphora*	50	13.30	1.24	9.3%	1.06	−0.22	1.02	7.6%
FRVEG	*Fraxinus velutina modesto*	36	11.86	1.25	10.5%	1.06	−0.11	1.10	9.3%
GIBI	*Ginkgo biloba*	54	11.25	1.43	12.7%	1.04	0.74	0.83	7.4%
LAIN	*Lagerstroemia indica*	24	5.85	1.01	17.3%	0.99	0.58	0.88	15.0%
LIST	*Liquidambar styraciflua*	37	9.73	1.13	11.6%	1.06	−0.11	1.01	10.4%
LITU	*Liriodendron tulipifera*	46	12.73	1.46	11.5%	1.06	0.14	1.15	9.0%
MAGR	*Magnolia grandiflora*	58	10.31	1.34	12.9%	1.00	0.94	0.92	8.9%
PICH	*Pistacia chinensis*	34	12.23	1.63	13.4%	0.93	1.62	1.35	11.0%
PLAC	*Platanus × acerifolia*	41	13.82	1.34	9.7%	0.98	0.93	1.16	8.4%
PRCE	*Prunus cerasifera* spp.	19	6.63	1.18	17.9%	0.82	1.77	0.91	13.7%
PYCA	*Pyrus calleryana* spp.	30	8.32	0.96	11.5%	1.12	−0.32	0.62	7.5%
QUAG1	*Quercus agrifolia*	45	12.18	1.86	15.2%	1.08	0.59	1.02	8.4%
QULO	*Quercus lobata*	44	14.19	1.43	10.1%	1.03	0.69	0.94	6.6%
QURU	*Quercus rubra*	32	12.45	1.05	8.4%	1.02	0.26	0.90	7.3%
SESE	*Sequoia sempervirens*	41	7.95	0.89	11.2%	1.03	0.21	0.78	9.9%
ULPA	*Ulmus parvifolia*	47	16.31	1.67	10.2%	1.03	0.74	1.16	7.1%
ZESE	*Zelkova serrata*	38	14.29	1.41	9.9%	1.06	−0.03	1.12	7.8%
All		802	11.95	1.43	12.0%			1.07	9.0%

3.2. Regression models: DBH estimation from crown diameter

Allometric equations were established between field-measured DBH and crown diameters to estimate DBH from crown diameters measured using the NAIP images. Table 5 shows goodness of fit for the three different models tested. Although we used RMSEs to determine the best model, the results indicated that the differences of RMSE values among the three models were very small. In other words, selecting the best model within the three different models was not critical to improve the model's accuracy. Instead, including

Table 5
Regression models for DBH estimation from field measured crown diameters.

Species	Models	RMSE (cm)	RMSE (%)	r^2
CEDE	$dbh = 5.68 \times CD - 8.03$	10.00	15.3%	0.911
	$sqrt(dbh) = 2.55 \times sqrt(CD) - 1.10$	9.97	15.3%	0.911
	$dbh = 3.57 \times CD^{1.13}$	9.99	15.3%	0.911
CEOC	$dbh = 3.82 \times CD - 5.48$	8.60	20.8%	0.834
	$sqrt(dbh) = 2.07 \times sqrt(CD) - 0.85$	8.39	20.3%	0.843
	$dbh = 2.51 \times CD^{1.11}$	9.92	24.0%	0.780
CESI4	$dbh = 4.99 \times CD - 14.91$	11.27	21.7%	0.827
	$sqrt(dbh) = 2.66 \times sqrt(CD) - 2.59$	10.99	21.2%	0.835
	$dbh = 1.44 \times CD^{1.37}$	10.99	21.2%	0.835
CICA	$dbh = 5.18 \times CD - 7.83$	10.77	17.6%	0.898
	$sqrt(dbh) = 2.43 \times sqrt(CD) - 1.09$	10.70	17.5%	0.899
	$dbh = 3.23 \times CD^{1.13}$	11.09	18.2%	0.892
FRVEG	$dbh = 4.98 \times CD + 0.35$	16.64	28.0%	0.688
	$sqrt(dbh) = 2.22 \times sqrt(CD) + 0.06$	16.58	27.9%	0.690
	$dbh = 5.10 \times CD^{0.99}$	17.00	28.6%	0.674
GIBI	$dbh = 4.60 \times CD - 4.20$	11.15	23.4%	0.772
	$sqrt(dbh) = 2.27 \times sqrt(CD) - 0.72$	11.10	23.3%	0.774
	$dbh = 3.21 \times CD^{1.11}$	11.18	23.5%	0.771
LAIN	$dbh = 3.39 \times CD + 0.79$	6.46	31.3%	0.570
	$sqrt(dbh) = 1.81 \times sqrt(CD) + 0.18$	6.48	31.4%	0.568
	$dbh = 3.79 \times CD^{0.96}$	6.50	31.5%	0.565
LIST	$dbh = 4.99 \times CD - 4.06$	8.15	18.3%	0.888
	$sqrt(dbh) = 2.33 \times sqrt(CD) - 0.63$	8.14	18.3%	0.889
	$dbh = 3.77 \times CD^{1.08}$	8.22	18.5%	0.886
LITU	$dbh = 5.62 \times CD - 11.52$	9.99	16.7%	0.903
	$sqrt(dbh) = 2.65 \times sqrt(CD) - 1.77$	9.78	16.3%	0.907
	$dbh = 2.57 \times CD^{1.23}$	9.95	16.6%	0.904
MAGR	$dbh = 5.62 \times CD - 8.39$	8.88	17.9%	0.831
	$sqrt(dbh) = 2.61 \times sqrt(CD) - 1.37$	8.84	17.8%	0.832
	$dbh = 3.03 \times CD^{1.19}$	8.94	18.0%	0.828
PICH	$dbh = 3.64 \times CD - 4.47$	5.83	14.6%	0.889
	$sqrt(dbh) = 1.99 \times sqrt(CD) - 0.64$	6.03	15.1%	0.882
	$dbh = 2.67 \times CD^{1.08}$	5.98	14.9%	0.884
PLAC	$dbh = 4.63 \times CD - 5.97$	11.62	20.7%	0.871
	$sqrt(dbh) = 2.25 \times sqrt(CD) - 0.77$	11.74	20.9%	0.868
	$dbh = 3.27 \times CD^{1.09}$	11.71	20.9%	0.869
PRCE	$dbh = 2.79 \times CD + 8.33$	7.66	28.5%	0.591
	$sqrt(dbh) = 1.35 \times sqrt(CD) + 1.72$	7.61	28.4%	0.595
	$dbh = 7.90 \times CD^{0.65}$	7.45	27.7%	0.600
PYCA	$dbh = 3.53 \times CD + 0.80$	5.05	16.8%	0.863
	$sqrt(dbh) = 1.85 \times sqrt(CD) + 0.15$	5.02	16.7%	0.864
	$dbh = 3.84 \times CD^{0.97}$	5.14	17.1%	0.858
QUAG1	$dbh = 4.35 \times CD - 4.80$	6.46	13.7%	0.915
	$sqrt(dbh) = 2.16 \times sqrt(CD) - 0.60$	6.71	14.2%	0.908
	$dbh = 3.32 \times CD^{1.07}$	6.56	13.9%	0.913
QULO	$dbh = 5.53 \times CD - 17.48$	16.33	27.3%	0.804
	$sqrt(dbh) = 2.80 \times sqrt(CD) - 2.86$	16.22	27.1%	0.807
	$dbh = 1.59 \times CD^{1.36}$	16.53	27.6%	0.799
QURU	$dbh = 3.87 \times CD - 6.57$	8.24	19.7%	0.899
	$sqrt(dbh) = 2.20 \times sqrt(CD) - 1.39$	8.00	19.1%	0.905
	$dbh = 1.87 \times CD^{1.21}$	7.80	18.6%	0.910
SESE	$dbh = 11.47 \times CD - 22.00$	17.03	24.6%	0.877
	$sqrt(dbh) = 3.95 \times sqrt(CD) - 2.93$	16.86	24.4%	0.879
	$dbh = 4.23 \times CD^{1.33}$	18.13	26.2%	0.860
ULPA	$dbh = 3.61 \times CD - 4.60$	10.21	18.8%	0.780
	$sqrt(dbh) = 1.97 \times sqrt(CD) - 0.61$	10.25	18.9%	0.778
	$dbh = 2.71 \times CD^{1.07}$	10.28	18.9%	0.777
ZESE	$dbh = 4.31 \times CD - 6.75$	12.29	23.2%	0.820
	$sqrt(dbh) = 2.17 \times sqrt(CD) - 0.83$	12.38	23.3%	0.818
	$dbh = 3.09 \times CD^{1.08}$	12.60	23.7%	0.811
Total	Species−specific model	10.80	21.1%	0.872
No species info	$dbh = 4.51 \times CD - 2.05$	17.58	33.5%	0.693
	$sqrt(dbh) = 2.15 \times sqrt(CD) - 0.25$	17.63	33.6%	0.693
	$dbh = 4.07 \times CD^{1.03}$	17.59	33.5%	0.693

species information improved the accuracy of the DBH estimation from the crown diameter. When species information was excluded the RMSE of all trees for estimating DBH was 17.6 cm (33.6%). However, when species information was included the RMSE of all trees decreased to 10.8 cm (21.1%). Square-root transformed models (Eq. (2)) were selected as the best models for most species (13 out of 20 species). For cherry plum (*Prunus cerasifera* spp., PRCE) and California white oak (*Q. lobata*, QULO), the non-linear power function (Eq. (3)) showed the best goodness of fit among 3 models. The linear model showed the best fit for Chinese pistache (*Pistacia chinensis*, PICH), London planetree (*Platanus* × *acerifolia*, PLAN), coastal live oak (*Quercus agrifolia*, QUAG1), Chinese elm (*Ulmus parvifolia*, ULPA), and Japanese zelkova (*Zelkova serrata*, ZESE). However, for most species, only a small improvement over the other models.

3.3. Stem diameter (DBH) estimation accuracy

The relative RMSE (%) of DBH_{ap} was larger than that of CD_{ap}, possibly because the errors were compounded when we estimated the crown measurements from aerial images and applied the regression model. Fig. 5(b) shows the relationship between field-measured DBH and estimated DBH using aerial image. As Table 6 shows, the absolute RMSE of estimated DBH_{ap} for all 20 species was 10.32 cm (20.2%). As expected, absolute RMSEs (cm) show a positive relationship with the DBH (the species with larger DBHs have larger RMSEs) while trees with smaller DBH tended to have larger RMSE percentage values. The small crape myrtle (*L. indica*, LAIN) showed small RMSE (5.31 cm) among 20 species and relatively large RMSE (25.7%) in percentage value. Although Modesto ash (*Fraxinus velutina modesto*, FRVEG) and California white oak (*Q. lobata*, QULO) are larger species, both species showed relatively large RMSE (26.1% and 25.1%, respectively). In other words, estimated DBHs using crown radius were less accurate, compared to the other species due to the uncertainties in the regression models that used crown diameters to estimate DBHs.

3.4. Height estimation accuracy

Previous studies reported a tendency to underestimate tree height using LiDAR (Andersen et al., 2006; Gaveau and Hill, 2003; McCombs et al., 2003; Nilsson, 1996), and our initial result using the LiDAR data also underestimated tree height. In addition to the well-known characteristics of airborne discrete LiDAR sensors (failing to record treetops due to insufficient sampling density) and the rasterization process with smoothing, this might have been because of the time gap between the LiDAR survey (2007 and 2008) than the field survey conducted a few years later (2010 and 2012). We adjusted the underestimated tree heights by adding a different value for each species as an offset (Eq. (5)). To quantify the adjusted height, we fixed the slope coefficient to 1 and calculated the bias (intercept) using the linear model. All tree species showed negative bias (i.e., underestimated height). Before the adjustment, the RMSE of mean tree height was 2.5 m (17.2%) and it decreased to 1.6 m (11.3%) after the adjustment (Table 7; Fig. 5(c)). The relationship between absolute RMSEs (m) and tree height (the species with larger tree heights have larger RMSEs) was weak, while trees with smaller height still tended to have larger RMSE percentage values. Among the 20 species, tulip tree (*Liriodendron tulipifera*, LITU) showed the smallest RMSE (8.31%) and common crape myrtle (*L. indica*, LAIN) showed the largest RMSE (22.16%).

$$HT_{adj} = 1 \times HT_{li} + \text{offset} \quad (5)$$

where HT_{adj} is the adjusted tree height and HT_{li} is the tree height from LiDAR.

3.5. Biomass estimation with crown diameter and tree height

Using tree dimensions estimated from the imagery, we calculated aboveground biomass for individual trees using species-specific biomass equations. The equations for deodar cedar (*C. deodara*), northern red oak (*Quercus rubra*), and coast redwood (*S. sempervirens*) produced dry weight values. The equations for the other 17 species produced wood volume values that were converted into dry weight using conversion factors for each species (Chave et al., 2009). Table 8 shows RMSE of biomass estimation with DBH-and-height models and with DBH-only models. In the case of *Q. agrifolia* and *Q. lobata*, biomass was calculated with only a DBH-and-height model. Biomass was calculated with a DBH-only model for deodar cedar (*C. deodara*), northern red oak (*Q. rubra*), and coast redwood (*S. sempervirens*). Biomass estimates from allometric equations that included tree height were more accurate than those from DBH-only equations. The RMSEs and R^2 values for DBH-and-height and DBH-only models were 799.2 and 0.88 and 919.8 and 0.85, respectively. Fig. 5(d) shows the relationship between allometric biomass from field measurements and the estimated biomass using measurements from remote sensing data for 20 species. Exceptions were found for common hackberry (*Celtis occidentalis*, CEOC) and Chinese hackberry (*Celtis sinensis*, CEIS4). Including tree height estimated from the LiDAR data for these two tall-growing species added relatively more error to their calculated biomass.

Biomass estimation errors tended to be influenced by DBH_{ap} and HT_{li} estimation errors. Tree species with larger errors in estimating dimensions tended to have larger errors in biomass estimation and vice versa. For example, Modesto ash (*F. velutina modesto*, FRVEG) and common crape myrtle (*L. indica*, LAIN) had relatively large RMSE values for estimates of both height and biomass.

4. Discussion

We evaluated the accuracy of using remotely sensed data to estimate the dimensions and biomass of individual street trees in an urban area. From the NAIP aerial photo images, we digitized crown boundaries on aerial photos and estimated approximate crown diameters (CD_{ap}). The accuracy of estimated crown diameters was tested using field-measured crown diameters. After adjustment the absolute RMSE of CD_{ap} estimation was 1.07 m (9.0%), and the relative RMSE (%) had a negative relationship with crown diameter (ranges from 6.6% to 15.0%). We also tested three regression models to estimate DBH from CD_{ap}, determined the best-fit model for each species, and tested the accuracy of estimated DBH_{ap} using field-measured DBH. The RMSE of DBH_{ap} estimation of all trees was 10.32 cm (20.2%). The relative RMSE (%) of DBH_{ap} was larger than for CD_{ap}, partly because of additional error introduced in the allometric model. We found that the DBH_{ap} estimation became more accurate if we accounted for species-dependent relationships between DBH and crown diameter. LiDAR surface models produced consistently low estimates of height. The RMSE of height estimates (HT_{li}) decreased from 2.5 m (17.1%) to 1.6 m (11.2%) after adding an offset value. Like the RMSE of crown diameter, the RMSE of tree heights showed a negative relationship with tree heights.

In this study, we adjusted both DBH and height estimations using field-based values to improve the accuracy of the biomass calculations. The RMSE of biomass estimation was 799.2 kg (44.8%) and R^2 was 0.881 with the DBH-and-height model. It is worth noting that without these adjustments, biomass estimates using tree dimensions (DBH_{ap} and HT_{li}) from remotely sensed data will be underestimated because both DBH_{ap} and HT_{li} dimensions are underestimated.

Table 6
RMSE of DBH estimation for 20 tree species with regression models and crown diameters from aerial imagery.

Species	Scientific name	# trees	Mean DBH (cm)	RMSE		r^2
				(cm)	(%)	
CEDE	*Cedrus deodara*	49	65.35	10.51	16.1%	0.901
CEOC	*Celtis occidentalis*	28	41.42	7.46	18.0%	0.875
CESI4	*Celtis sinensis*	49	51.94	9.26	17.8%	0.883
CICA	*Cinnamomum camphora*	50	61.06	11.66	19.1%	0.880
FRVEG	*Fraxinus velutina modesto*	36	59.37	15.52	26.1%	0.729
GIBI	*Ginkgo biloba*	54	47.54	10.25	21.6%	0.807
LAIN	*Lagerstroemia indica*	24	20.64	5.31	25.7%	0.710
LIST	*Liquidambar styraciflua*	37	44.52	8.74	19.6%	0.872
LITU	*Liriodendron tulipifera*	46	60.00	9.59	16.0%	0.911
MAGR	*Magnolia grandiflora*	58	49.57	10.58	21.3%	0.759
PICH	*Pistacia chinensis*	34	40.04	8.23	20.5%	0.780
PLAC	*Platanus × acerifolia*	41	56.08	11.77	21.0%	0.867
PRCE	*Prunus cerasifera* spp.	19	26.85	6.39	23.8%	0.449
PYCA	*Pyrus calleryana* spp.	30	30.14	4.54	15.1%	0.889
QUAG1	*Quercus agrifolia*	45	47.16	7.80	16.5%	0.876
QULO	*Quercus lobata*	44	59.93	15.03	25.1%	0.834
QURU	*Quercus rubra*	32	41.92	7.17	17.1%	0.924
SESE	*Sequoia sempervirens*	41	69.17	13.06	18.9%	0.928
ULPA	*Ulmus parvifolia*	47	54.33	9.29	17.1%	0.818
ZESE	*Zelkova serrata*	38	53.08	10.51	19.8%	0.869
Total		802	51.15	10.32	20.2%	0.883

Table 7
RMSE of tree height estimation of 20 tree species from LiDAR data.

Species	Scientific name	# trees	Before adjustment			After adjustment		
			Mean height	RMSE		Offset	RMSE	
			(m)	(m)	(%)		(m)	(%)
CEDE	*Cedrus deodara*	49	19.97	2.49	12.4%	1.71	1.88	9.4%
CEOC	*Celtis occidentalis*	28	11.48	1.65	14.4%	1.28	1.22	10.6%
CESI4	*Celtis sinensis*	49	12.30	2.53	20.6%	2.00	1.65	13.4%
CICA	*Cinnamomum camphora*	50	13.89	2.16	15.5%	1.48	1.63	11.8%
FRVEG	*Fraxinus velutina modesto*	36	12.70	2.08	16.4%	1.52	1.36	10.7%
GIBI	*Ginkgo biloba*	54	14.93	3.34	22.4%	2.85	1.75	11.7%
LAIN	*Lagerstroemia indica*	24	6.33	1.85	29.3%	1.18	1.43	22.7%
LIST	*Liquidambar styraciflua*	37	16.95	2.85	16.8%	2.39	1.65	9.7%
LITU	*Liriodendron tulipifera*	46	20.64	2.83	13.7%	2.34	1.81	8.8%
MAGR	*Magnolia grandiflora*	58	12.81	1.84	14.4%	1.21	1.45	11.3%
PICH	*Pistacia chinensis*	34	12.33	2.13	17.3%	1.70	1.34	10.8%
PLAC	*Platanus × acerifolia*	41	17.18	2.48	14.4%	1.86	1.79	10.4%
PRCE	*Prunus cerasifera* spp.	19	6.56	1.58	24.1%	0.55	1.66	25.3%
PYCA	*Pyrus calleryana* spp.	30	11.07	2.32	20.9%	1.86	1.68	15.1%
QUAG1	*Quercus agrifolia*	45	11.83	2.47	20.9%	1.69	1.69	14.3%
QULO	*Quercus lobata*	44	15.24	2.78	18.2%	2.18	1.68	11.0%
QURU	*Quercus rubra*	32	14.65	2.79	19.1%	2.39	1.57	10.7%
SESE	*Sequoia sempervirens*	41	19.24	2.94	15.3%	2.26	1.83	9.5%
ULPA	*Ulmus parvifolia*	47	15.43	2.56	16.6%	2.12	1.65	10.7%
ZESE	*Zelkova serrata*	38	13.89	2.51	18.1%	1.91	1.56	11.3%
All		802	14.50	2.50	17.2%		1.64	11.3%

There are several sources of error that influence the accuracy of tree biomass estimates from remote sensing. Correctly locating the target tree for measurement can be a source of error when the exact address and GPS location are not available. These data were available for sample trees in this study, but there was still a chance of selecting the wrong tree for measurement when target trees had crowns that were small, clumped together or under the crowns of taller trees.

The quality of imagery influenced errors associated with measuring crown diameter (Mäkinen et al., 2006). Although the NAIP imagery was ortho-rectified, not every object in the imagery was perfectly ortho-rectified. Some tree crowns appeared in perspective view rather than perpendicular view. Shadowed areas are problematic because they make it difficult to correctly delineate crown boundaries (Richardson and Moskal, 2014). To correctly locate trees and improve crown measurement accuracy it is important to acquire high-resolution imagery that was taken recently during the leaf-on season. Imagery with high spatial resolution (i.e., 15 to 30-cm resolution instead of NAIP's 1 m resolution) will improve the accuracy of crown diameter measurements and reduce the possibility of digitizing the incorrect tree's crown. In addition, the accuracy could be improved by applying the relief correction method to the aerial images (Lehrbass and Wang, 2012). If possible, extracting canopy diameter from leaf-on LiDAR data (instead of aerial imagery) will eliminate view geometry issues.

The three to four year time gap between the field survey (2010 and 2012) and LiDAR data acquisition (2007 and 2008) is another source of error. Tree heights were underestimated from LiDAR. The time gap and sensor accuracy contributed to this negative bias. Although the LiDAR sensor's accuracy is very high (vertical accuracy is less than 18.5 cm at 95% confidence level), it did not directly translate into accurate extraction of tree height. This study showed

Table 8
RMSE of tree above ground biomass estimation of 20 tree species with two types of models (DBH and height model, DBH only model).

Code	Scientific name	*n*	Mean volume	DW density factor	Mean biomass	RMSE			
						DBH-Height		DBH only	
			(m^3)		(kg)	(kg)	r^2	(kg)	r^2
CEDE[b]	*Cedrus deodara*	49	–	–	2268.4	840.8	0.856	840.8	0.856
CEOC	*Celtis occidentalis*	28	2.38	490	1168.3	533.4	0.716	478.0	0.772
CESI4	*Celtis sinensis*	49	3.82	490	1872.7	683.3	0.834	701.6	0.825
CICA	*Cinnamomum camphora*	50	4.44	520	2307.5	1073.7	0.838	1173.5	0.806
FRVEG	*Fraxinus velutina modesto*	36	3.07	510	1567.6	783.6	0.866	964.9	0.796
GIBI	*Ginkgo biloba*	54	3.17	520	1650.6	590.9	0.903	769.5	0.836
LAIN	*Lagerstroemia indica*	24	0.33	571	188.2	78.2	0.815	95.4	0.725
LIST	*Liquidambar styraciflua*	37	2.25	460	1033.5	583.7	0.846	681.6	0.791
LITU	*Liriodendron tulipifera*	46	6.26	470	2943.3	866.2	0.923	1247.4	0.840
MAGR	*Magnolia grandiflora*	58	1.98	460	909.3	404.9	0.766	634.4	0.426
PICH	*Pistacia chinensis*	34	1.67	685	1143.4	495.0	0.765	646.5	0.600
PLAC	*Platanus × acerifolia*	41	4.92	500	2459.4	1069.7	0.892	1074.5	0.891
PRCE	*Prunus cerasifera* spp.	19	0.49	470	231.3	84.3	0.598	104.4	0.383
PYCA	*Pyrus calleryana* spp.	30	0.99	600	596.7	177.1	0.864	188.5	0.846
QUAG1[a]	*Quercus agrifolia*	45	2.46	590	1873.5	511.9	0.887	–	–
QULO[a]	*Quercus lobata*	44	3.75	550	3223.3	1065.7	0.811	–	–
QURU[b]	*Quercus rubra*	32	–	–	1873.5	802.6	0.886	802.6	0.886
SESE[b]	*Sequoia sempervirens*	41	–	–	3223.3	1513.9	0.867	1513.9	0.867
ULPA	*Ulmus parvifolia*	47	3.52	730	2567.6	742.8	0.857	1248.8	0.597
ZESE	*Zelkova serrata*	38	3.60	520	1870.1	929.1	0.845	1034.6	0.807
All		802			1782.0	799.2	0.881	919.8	0.846

DW, dry weight.
[a] DBH-only model is not available (DBH-and-height is used).
[b] DBH-and-Height model is not available (DBH-only model is used).

how the negative bias in tree height estimation can be adjusted. The adjustment offset value can vary depending on tree species and the seasonality of data collection (i.e., leaf-on and leaf-off). We suggest that budgets for data collection include funds for photo interpretation training and field surveys to verify the remotely sensed data. Training and field validation should focus on the most challenging cases, such as clumped trees, large trees with shadows and small-stature tree species. With this information analysts are better able to make adjustments that correct spatial and temporal biases from remotely sensed data. Tree dimensions obtained from secondary and tertiary estimations tended to contain the largest errors. For example, estimating DBH required multiple steps and errors were propagated through each step: digitizing CPA, estimating crown diameter from CPA, estimating DBH from CPA and calculating biomass with DBH. Tree heights were estimated from the LiDAR data while DBH was estimated through multiple steps. This approach reduced error propagation. When multiple estimation steps are unavoidable, using a species-specific allometric model can significantly reduce the errors. We used allometrically estimated biomass as the references for our analysis and we did not quantify the discrepancy between the real biomass and allometrically estimated biomass. We did not have permission or capacity to harvest, measure and weigh trees to determine actual biomass. Most urban forest biomass estimation studies confront this limitation. It is worth noting that more accurate estimates are especially important for smaller-stature trees because their relative RMSEs were highest. However, tall trees contribute relatively more biomass to the city total than short trees. Also, it should be noted that the main objective of this study is to quantify the errors associated with estimating biomass using currently available remote sensing data at individual tree level. Future studies may be able to use results such as these to scale-up single-tree data to the larger urban forest.

5. Conclusions

We conclude that extracting urban tree dimensions from remotely sensed data has potential to supplement traditional field survey if key limitations are addressed. Acquiring high-resolution imagery taken during the leaf-on season is a critical starting point. Providing adequate photo interpretation training and field verification are essential to locating the correct trees and accurately measuring crown dimensions. Also, the use of automated methods such as described in this paper can reduce processing time required for tree crown segmentation. Reducing the number of steps taken to calculate tree dimensions and using species-specific allometric equations improve the accuracy of biomass estimates. Although we advise caution when applying the regression models developed in this study to areas where trees grow and are managed differently, concepts underpinning their derivation and application can be replicated elsewhere. For example, this approach can be incorporated into urban forest carbon project protocols (e.g., California's *Urban Forest Project Protocol* by Climate Action Reserve, 2010) to customize allometric equations for locally important tree species and expedite monitoring and quantification of carbon stocks.

Acknowledgements

We gratefully acknowledge the USDA Forest Service Pacific Southwest Research Station (Prime Award No. 12-CA-11272131-045; Sub-agreement No. 00008201) for funding this project. We deeply thank Paula Peper for providing the allometric equations and field measurement data. We also thank Shannon Albers and Jose Martinez for field work. Lastly we thank Professor John D. Radke of the University of California at Berkeley for his support in administering this project.

References

Aguaron, E., McPherson, E.G., 2012. Comparison of methods for estimating carbon dioxide storage by Sacramento's urban forest. In: Carbon Sequestration in Urban Ecosystems. Springer, Dordrecht, Netherlands, pp. 43–71.

Alonzo, M., Bookhagen, B., McFadden, J.P., Sun, A., Roberts, D.A., 2015. Mapping urban forest leaf area index with airborne lidar using penetration metrics and allometry. Remote Sens. Environ. 162, 141–153, http://dx.doi.org/10.1016/j.rse.2015.02.025.

Alonzo, M., Bookhagen, B., Roberts, D.A., 2014. Urban tree species mapping using hyperspectral and lidar data fusion. Remote Sens. Environ. 148, 70–83, http://dx.doi.org/10.1016/j.rse.2014.03.018.

American Forests, 2014. Sacramento Urban Forest Fact Sheet [WWW Document] (accessed 6.13.14) http://www.americanforests.org/our-programs/urbanforests/10-best-cities-for-urban-forests/10-best-cities-for-urban-forests-sacramento/sacramento-urban-forest-fact-sheet/.
Andersen, H.-E., Reutebuch, S.E., McGaughey, R.J., 2006. A rigorous assessment of tree height measurements obtained using airborne lidar and conventional field methods. Can. J. Remote Sens. 32, 355–366.
Anderson, L.M., Cordell, H.K., 1988. Influence of trees on residential property values in Athens, Georgia (USA): a survey based on actual sales prices. Landscape Urban Plan. 15, 153–164.
Anderson-Sprecher, R., 1994. Model comparisons and R^2. Am. Stat. 48, 113, http://dx.doi.org/10.2307/2684259.
Chave, J., David, C., Steven, J., Simon, L.L., Nathan, G.S., Amy, E.Z., 2009. Towards a worldwide wood economics spectrum. Ecol. Lett. 12, 351–366.
Chen, Q., Baldocchi, D., Gong, P., Kelly, M., 2006. Isolating individual trees in a Savanna woodland using small footprint lidar data. Photogramm. Eng. Remote Sens. 72, 923–932.
Chen, Q., Gong, P., Baldocchi, D., Tian, Y.Q., 2007. Estimating basal area and stem volume for individual trees from lidar data. Photogramm. Eng. Remote Sens. 73, 1355.
City of Sacramento, 2012. About the City of Sacramento [WWW Document]. http://www.cityofsacramento.org/about_the_city.htm.
Culvenor, D.S., 2002. TIDA: an algorithm for the delineation of tree crowns in high spatial resolution remotely sensed imagery. Comput. Geosci. 28, 33–44.
Dawkins, H.S., 1963. Crown diameters: their relation to bole diameter in tropical forest trees. Commonw. Forest. Rev. 42, 318–333.
Deng, C., Wu, C., 2013. Examining the impacts of urban biophysical compositions on surface urban heat island: a spectral unmixing and thermal mixing approach. Remote Sens. Environ. 131, 262–274, http://dx.doi.org/10.1016/j.rse.2012.12.020.
Donovan, G.H., Butry, D.T., 2009. The value of shade: estimating the effect of urban trees on summertime electricity use. Energy Build. 41, 662–668.
Donovan, G.H., Butry, D.T., Michael, Y.L., Prestemon, J.P., Liebhold, A.M., Gatziolis, D., Mao, M.Y., 2013. The relationship between trees and human health. Am. J. Prev. Med. 44, 139–145, http://dx.doi.org/10.1016/j.amepre.2012.09.066.
Dralle, K., Rudemo, M., 1997. Automatic estimation of individual tree positions from aerial photos. Can. J. For. Res. 27, 1728–1736.
Draper, N.R., 1998. Applied Regression Analysis, 3rd ed. Wiley Series in Probability and Statistics. Wiley, New York.
Enquist, B.J., 2002. Universal scaling in tree and vascular plant allometry: toward a general quantitative theory linking plant form and function from cells to ecosystems. Tree Physiol. 22, 1045–1064.
Gaveau, D.L., Hill, R.A., 2003. Quantifying canopy height underestimation by laser pulse penetration in small-footprint airborne laser scanning data. Can. J. Remote Sens. 29, 650–657.
Gidlöf-Gunnarsson, A., Öhrström, E., 2007. Noise and well-being in urban residential environments: the potential role of perceived availability to nearby green areas. Landscape Urban Plan. 83, 115–126, http://dx.doi.org/10.1016/j.landurbplan.2007.03.003.
Gong, P., Biging, G.S., Lee, S.M., Mei, X., Sheng, Y., Pu, R., Xu, B., Schwarzr, K.-P., Mostafa, M., 1999. Photo ecometrics for forest inventory. Geogr. Inform. Sci. 5, 9–14.
Gougeon, F.A., 1995. A crown-following approach to the automatic delineation of individual tree crowns in high spatial resolution aerial images. Can. J. Remote Sens. 21, 274–284.
Gougeon, F.A., Leckie, D.G., 2006. The individual tree crown approach applied to Ikonos images of a coniferous plantation area. Photogramm. Eng. Remote Sens. 72, 1287–1297.
Hemery, G.E., Savill, P.S., Pryor, S.N., 2005. Applications of the crown diameter–stem diameter relationship for different species of broadleaved trees. Forest Ecol. Manage. 215, 285–294.
Huang, Y.J., Akbari, H., Taha, H., Rosenfeld, A.H., 1987. The potential of vegetation in reducing summer cooling loads in residential buildings. J. Clim. Appl. Meteorol. 26, 1103–1116.
Hyyppä, J., Hyyppä, H., Leckie, D., Gougeon, F., Yu, X., Maltamo, M., 2008. Review of methods of small-footprint airborne laser scanning for extracting forest inventory data in boreal forests. Int. J. Remote Sens. 29, 1339–1366, http://dx.doi.org/10.1080/01431160701736489.
Hyyppä, J., Hyyppä, H., Litkey, P., Yu, X., Haggrén, H., Rönnholm, P., Pyysalo, U., Pitkänen, J., Maltamo, M., 2004. Algorithms and methods of airborne laser-scanning for forest measurements. Int. Arch. Photogramm. Remote Sens. Spat. Inf. Sci. 36, 1682–1750.
Jenkins, J.C., Chojnacky, D.C., Heath, L.S., Birdsey, R.A., 2003. National-scale biomass estimators for United States tree species. Forest Sci. 49, 12–35.
Jenkins, J.C., Chojnacky, D.C., Heath, L.S., Birdsey, R.A., 2004. Comprehensive database of diameter-based biomass regressions for North American tree species. GTR NE-319. USDA Forest Service, Northeastern.
Kalliovirta, J., Tokola, T., 2005. Functions for estimating stem diameter and tree age using tree height, crown width and existing stand database information. Silva Fenn. 39, 227–248.
Kaplan, R., Kaplan, S., 1989. The Experience of Nature: A Psychological Perspective. CUP Archive.
Ke, Y., Quackenbush, L.J., 2011. A review of methods for automatic individual tree-crown detection and delineation from passive remote sensing. Int. J. Remote Sens. 32, 4725–4747.
Kleinbaum, K., Nizam, M., 2008. Applied Regression Analysis and Other Multivariable Methods, 4th ed.
Koch, B., Dees, M., 2008. Forestry applications. In: Advances in Photogrammetry, Remote Sensing and Spatial Information Sciences., pp. 439–465.
Korpela, I., 2004. Individual tree measurements by means of digital aerial photogrammetry. Silva Fenn. 3, 1–93.
Korpela, I., Dahlin, B., Schäfer, H., Bruun, E., Haapaniemi, F., Honkasalo, J., Ilvesniemi, S., Kuutti, V., Linkosalmi, M., Mustonen, J., 2007. Single-tree forest inventory using lidar and aerial images for 3D treetop positioning, species recognition, height and crown width estimation. Int. Arch. Photogramm. Remote Sens. Spat. Inf. Sci. 36, 227–233.
Ko, Y., Radke, J.D., 2014. The effect of urban form on residential cooling energy use: the case of Sacramento, California. Environ. Plann. B: Plann. Des. 41, 573–593.
Kuo, F.E., Sullivan, W.C., 2001. Environment and crime in the inner city does vegetation reduce crime? Environ. Behav. 33, 343–367.
Kwak, D.-A., Lee, W.-K., Lee, J.-H., Biging, G.S., Gong, P., 2007. Detection of individual trees and estimation of tree height using LiDAR data. J. For. Res. 12, 425–434, http://dx.doi.org/10.1007/s10310-007-0041-9.
Larsen, M., Rudemo, M., 1998. Optimizing templates for finding trees in aerial photographs. Pattern Recogn. Lett. 19, 1153–1162.
Lee, J.H., 2010. Automated Approaches for Extracting Individual Tree Level Forest Information using High Spatial Resolution Remotely Sensed Data. University of California, Berkeley.
Lefsky, M., McHale, M.R., 2008. Volume estimates of trees with complex architecture from terrestrial laser scanning. J. Appl. Remote Sens. 2, 023521.
Lehrbass, B., Wang, J., 2012. Urban tree cover mapping with relief-corrected aerial imagery and lidar. Photogramm. Eng. Remote Sens. 78, 473–484, http://dx.doi.org/10.14358/PERS.78.5.473.
Lim, K., Treitz, P., Wulder, M., St-Onge, B., Flood, M., 2003. LiDAR remote sensing of forest structure. Prog. Phys. Geogr. 27, 88.
Lockhart, B.R., Weih Jr., R.C., Smith, K.M., 2005. Crown radius and diameter at breast height relationships for six bottomland hardwood species. J. Ark. Acad. Sci. 59, 110–115.
Mäkinen, A., Korpela, I., Tokola, T., Kangas, A., 2006. Effects of imaging conditions on crown diameter measurements from high-resolution aerial images. Can. J. For. Res. 36, 1206–1217.
McCombs, J.W., Roberts, S.D., Evans, D.L., 2003. Influence of fusing lidar and multispectral imagery on remotely sensed estimates of stand density and mean tree height in a managed loblolly pine plantation. Forest Sci. 49, 457–466.
McHale, M.R., Burke, I.C., Lefsky, M.A., Peper, P.J., McPherson, E.G., 2009. Urban forest biomass estimates: is it important to use allometric relationships developed specifically for urban trees? Urban Ecosyst. 12, 95–113, http://dx.doi.org/10.1007/s11252-009-0081-3.
McHale, M.R., McPherson, E.G., Burke, I.C., 2007. The potential of urban tree plantings to be cost effective in carbon credit markets. Urban For. Urban Gree. 6, 49–60.
McPherson, E.G., 1998. Atmospheric carbon dioxide reduction by Sacramento's urban forest. J. Arboric. 24, 215–223.
McPherson, E.G., 1994. Cooling Urban Heat Islands with Sustainable Landscapes. The Ecological City: Preserving and Restoring Urban Biodiversity. University of Massachusetts Press, Amherst, pp. 151–171.
McPherson, E.G., Luttinger, N., 1998. From nature to nurture: the history of Sacramento's urban forest. J. Arboric. 24, 72–88.
McPherson, E.G., Muchnick, J., 2005. Effect of street tree shade on asphalt concrete pavement performance. J. Arboric. 31, 303.
McPherson, E.G., Peper, P.J., 2012. Urban tree growth modeling. Arboric. Urb. Forest. 38, 175–183.
McPherson, E.G., Rowntree, R.A., 1993. Energy conservation potential of urban tree planting. J. Arboric. 19, 321.
McPherson, E.G., Rowntree, R.A., 1988. Geometric solids for simulation of tree crowns. Landscape Urban Plan. 15, 79–83.
McPherson, E.G., Xiao, Q., Aguaron, E., 2013. A new approach to quantify and map carbon stored, sequestered and emissions avoided by urban forests. Landscape Urban Plan. 120, 70–84, http://dx.doi.org/10.1016/j.landurbplan.2013.08.005.
Morani, A., Nowak, D.J., Hirabayashi, S., Calfapietra, C., 2011. How to select the best tree planting locations to enhance air pollution removal in the Million Trees NYC initiative. Environ. Pollut. 159, 1040–1047, http://dx.doi.org/10.1016/j.envpol.2010.11.022.
Mugo, J.M., Njunge, J.T., Malimbwi, R.E., Kigomo, B.N., Mwasi, B.N., Muchiri, M.N., 2011. Models for predicting stem diameter from crown diameter of open grown trees in Sondu-Nyando River Catchment, Kenya. Asian J. Agric. Sci., 3.
Niklas, K.J., 1994. Plant Allometry: The Scaling of Form and Process. University of Chicago Press.
Nilsson, M., 1996. Estimation of tree heights and stand volume using an airborne lidar system. Remote Sens. Environ. 56, 1–7.
Nowak, D.J., 1993. Historical vegetation change in Oakland and its implications for urban forest management. J. Arboric. 19, 313–319.
Nowak, D.J., Crane, D.E., 2002. Carbon storage and sequestration by urban trees in the USA. Environ. Pollut. 116, 381–389.
Nowak, D.J., Crane, D.E., Stevens, J.C., 2006. Air pollution removal by urban trees and shrubs in the United States. Urban For. Urban Gree. 4, 115–123, http://dx.doi.org/10.1016/j.ufug.2006.01.007.
Nowak, D.J., Greenfield, E.J., 2012. Tree and impervious cover change in US cities. Urban For. Urban Gree. 11, 21–30.
Nowak, D.J., Greenfield, E.J., Hoehn, R.E., Lapoint, E., 2013. Carbon storage and sequestration by trees in urban and community areas of the United States.

Environ. Pollut. 178, 229–236, http://dx.doi.org/10.1016/j.envpol.2013.03.019.
Parlin, M., 2009. Seattle, Washington Urban Tree Canopy Analysis Project Report: Looking Back and Moving Forward. Native Communities Development Corporation, Colorado Springs.
Peper, P.J., McPherson, E.G., Mori, S.M., 2001a. Predictive equations for dimensions and leaf area of coastal Southern California street trees. J. Arboric. 27, 169–180.
Peper, P.J., McPherson, E.G., Mori, S.M., 2001b. Equations for predicting diameter, height, crown width, and leaf area of San Joaquin Valley street trees. J. Arboric. 27, 306–317.
Popescu, S.C., 2007. Estimating biomass of individual pine trees using airborne lidar. Biomass Bioenergy 31, 646–655.
Popescu, S.C., Wynne, R.H., 2004. Seeing the trees in the forest: using lidar and multispectral data fusion with local filtering and variable window size for estimating tree height. Photogramm. Eng. Remote Sens. 70, 589–604.
Pillsbury, N.H., Kirkley, M.L., 1984. Equations for total, wood, and saw-log volume for thirteen California hardwoods.
Pillsbury, N.H., Jeffrey, L.R., Richard, P.T., 1998. Tree Volume Equations for Fifteen Urban Species in California. Urban Forest Ecosystems Institute, California Polytechnic State University, San Luis Obispo, CA.
Richardson, J.J., Moskal, L.M., 2014. Uncertainty in urban forest canopy assessment: lessons from Seattle, WA, USA. Urban For. Urban Gree. 13, 152–157, http://dx.doi.org/10.1016/j.ufug.2013.07.003.
Roberts, D.A., Quattrochi, D.A., Hulley, G.C., Hook, S.J., Green, R.O., 2012. Synergies between VSWIR and TIR data for the urban environment: an evaluation of the potential for the Hyperspectral Infrared Imager (HyspIRI) Decadal Survey mission. Remote Sens. Environ. 117, 83–101, http://dx.doi.org/10.1016/j.rse.2011.07.021.
Rowntree, R.A., Nowak, D.J., 1991. Quantifying the role of urban forests in removing atmospheric carbon dioxide. J. Arboric. 17, 269–275.
Rozeboom, W.W., 1978. Estimation of cross-validated multiple correlation: a clarification. Psychol. Bull. 85, 1348–1351, http://dx.doi.org/10.1037/0033-2909.85.6.1348.
Sander, H., Polasky, S., Haight, R.G., 2010. The value of urban tree cover: a hedonic property price model in Ramsey and Dakota Counties, Minnesota, USA. Ecol. Econ. 69, 1646–1656.
Schroeder, H.W., Anderson, L.M., 1984. Perception of personal safety in urban recreation sites. J. Leis. Res. 16, 178–194.
Scott, K.I., McPherson, E.G., Simpson, J.R., 1998. Air pollutant uptake by Sacramento's urban forest. J. Arboric. 24, 224–234.
Shashua-Bar, L., Pearlmutter, D., Erell, E., 2011. The influence of trees and grass on outdoor thermal comfort in a hot-arid environment. Int. J. Climatol. 31, 1498–1506.
Shrestha, R., Wynne, R.H., 2012. Estimating biophysical parameters of individual trees in an urban environment using small footprint discrete-return imaging lidar. Remote Sens. 4, 484–508, http://dx.doi.org/10.3390/rs4020484.
Simpson, J.R., McPherson, E.G., 1998. Simulation of tree shade impacts on residential energy use for space conditioning in Sacramento. Atmos. Environ. 32, 69–74.
Spurr, S.H., 1960. Photogrammetry and photo-interpretation. Soil Sci. 90, 380.
Stone, M., 1974. Cross-validatory choice and assessment of statistical predictions. J. R. Stat. Soc. Ser. B: Methodol. 36, 111–147.
Ter-Mikaelian, M.T., Korzukhin, M.D., 1997. Biomass equations for sixty-five North American tree species. Forest Ecol. Manage. 97 (1), 1–24.
US Census Bureau, 2014. Sacramento (city) QuickFacts from the US Census Bureau [WWW Document] (accessed 6.13.14) http://quickfacts.census.gov/qfd/states/06/0664000.html.
van den Berg, A.E., Maas, J., Verheij, R.A., Groenewegen, P.P., 2010. Green space as a buffer between stressful life events and health. Soc. Sci. Med. 70, 1203–1210, http://dx.doi.org/10.1016/j.socscimed.2010.01.002.
Wang, L., Gong, P., Biging, G.S., 2004. Individual tree-crown delineation and treetop detection in high-spatial-resolution aerial imagery. Photogramm. Eng. Remote Sens. 70, 351–358.
Weng, Q., 2009. Thermal infrared remote sensing for urban climate and environmental studies: methods, applications, and trends. ISPRS J. Photogramm. Remote Sens. 64, 335–344, http://dx.doi.org/10.1016/j.isprsjprs.2009.03.007.
West, G.B., Brown, J.H., Enquist, B.J., 1999. A general model for the structure and allometry of plant vascular systems. Nature 400, 664–667.
Wilkinson, D.M., 1995. Modelling tree crowns as geometric solids. Arboric. J. 19, 387–393, http://dx.doi.org/10.1080/03071375.1995.9747085.
Wulder, M., Niemann, K.O., Goodenough, D.G., 2000. Local maximum filtering for the extraction of tree locations and basal area from high spatial resolution imagery. Remote Sens. Environ. 73, 103–114, http://dx.doi.org/10.1016/S0034-4257(00)00101-2.
Xiao, Q., McPherson, E.G., Simpson, J.R., Ustin, S.L., 1998. Rainfall interception by Sacramento's urban forest. J. Arboric. 24, 235–244.
Zhang, L., 1997. Cross-validation of non-linear growth functions for modelling tree height–diameter relationships. Ann. Bot. 79, 251–257, http://dx.doi.org/10.1006/anbo.1996.0334.